ORIGINAL ARTICLE

Studying the Innate Immune Response to Myocardial Infarction in a Highly Efficient Experimental Animal Model

Razvan Gheorghita MARES[1], Doina MANU[2], Istvan Adorjan SZABO[1], Mihaela Elena TOMUT[3], Gabriela PINTICAN[4], Bogdan CORDOS[1], Gabriel JAKOBSSON[5], Minodora DOBREANU[1,2,4], Ovidiu Simion COTOI[1,3], Alexandru SCHIOPU[1,5]

ABSTRACT

The reduction in mortality following acute myocardial infarction (AMI) is an important achievement of modern medicine. Despite this progress, AMI remains the most common cause of heart failure (HF) and HF-related morbidity and mortality. The involvement of the innate immune response in different stages after AMI has attracted important attention in recent years. With the increasing range of potential therapeutic compounds and delivery vectors, the need of highly efficient experimental AMI models is increasing, to support further advancement in this field. Here, we present a high-throughput model for the assessment of the innate immune response to AMI. The model is based on permanent surgical ligation of the left descending coronary artery (LAD) in mice, followed by complex flow-cytometry and histological analyses of immune cellular populations in blood and myocardium. We are presenting time-dependent qualitative and quantitative analysis results, demonstrating intense accumulation of Ly6G^{hi} neutrophils and Ly6C^{hi} monocytes in the infarcted myocardium on days 1 and 3 post-AMI, followed by successive accumulation of reparatory Ly6C^{lo}MerTK^{hi} macrophages, neovascularization and fibrosis development by day 7.

Keywords: acute myocardial infarction, experimental model, innate immunity, neutrophils, monocytes, macrophages, myocardial fibrosis, revascularization.

REZUMAT

Scăderea mortalității în urma infarctului miocardic acut (IMA) este o realizare remarcabilă a medicinei moderne. În ciuda acestui progres, IMA rămâne cea mai frecventă cauză a insuficienței cardiace (IC) și a morbidității și mortalității legate de IC. Implicarea răspunsului imun înnăscut în patologia IMA a atras o atenție deosebită în ultimii ani. Odată cu creșterea numărului de compuși cu potențial terapeutic, nevoia de modele experimentale eficiente de inducere a IMA este importantă, pentru a sprijini progresul în acest domeniu. Lucrarea de față prezintă un model de mare randament pentru evaluarea răspunsului imun înnăscut după IMA. Modelul se bazează pe ligaturarea chirurgicală permanentă a arterei descendente anterioare (ADA) la șoareci, urmată de analiză complexă de citometrie în flux și analiză histologică a populațiilor de celule imune din sânge și miocard. Prezentăm de asemenea rezultatele analizei calitative și cantitative în dinamică, demonstrând acumularea intensă a neutrofilelor Ly6G^{hi} și a monocitelor Ly6C^{hi} în miocardul infarctizat în zilele 1 și 3 post-IMA, urmată de acumularea succesivă de macrofage reparatorii Ly6C^{lo}MerTK^{hi}, neovascularizație și dezvoltarea fibrozei până în ziua a 7-a.

Cuvinte cheie: infarct miocardic acut, model experimental, imunitate înnăscută, neutrofile, monocite, macrophage, fibroză miocardică, revascularizare.

[1] „George Emil Palade" University of Medicine, Pharmacy, Science and Technology, Targu Mures, Romania
[2] Center for Advanced Medical and Pharmaceutical Research, Targu Mures, Romania
[3] Clinical County Hospital, Targu Mures, Romania
[4] Emergency Clinical County Hospital, Targu Mures, Romania
[5] Department of Clinical Sciences Malmö, Lund University, Sweden

Contact address:
Razvan Gheorghita MARES, 38 Gheorghe Marinescu Street, 540142, Targu Mures, Romania.
E-mail: razvan.mares@umfst.ro

1. INTRODUCTION

Acute myocardial infarction (AMI) is the most severe manifestation of coronary artery disease, causing more than a third of deaths in developed nations annually[1]. Although advances in critical care, pharmacological interventions and emergency management of AMI by timely reperfusion therapy have significantly reduced acute mortality in AMI, surviving patients remain at high risk to develop heart failure (HF)[2]. Thus, there is an urgent need for a better understanding of the pathogenesis of cardiomyocyte death, cardiac dysfunction and ventricular remodeling, in view of further development of novel therapeutic approaches.

Animal models of ischemic heart disease hold great importance, both in exploring novel mechanisms and for the development of future successful therapeutic interventions that can be clinically translated. Despite alternative AMI models that have been proposed and studied during recent years, including chemical[3], radiofrequency[4], thermal[5] or cryogenic injuries[6], permanent left descending coronary artery (LAD) occlusion remains the most common model used by researchers[7].

Classically, a ventilation-based thoracotomy to induce AMI by left descending coronary artery (LAD) ligation in mice was first introduced by Johns and Olson in 1954, in which substantial animal trauma and tissue damage are involved in order to reach the ischemic event[8]. This procedure is extremely labor intensive and time-consuming, and is associated with high surgery-related mortality, due at least in part to the trauma caused by intubation and mechanical ventilation, and to the large intercostal thoracotomy. To alleviate these problems, Gao et al. substantially improved the method by eliminating the need for mechanical ventilation and orotracheal intubation, using a minimally invasive approach[9].

In this paper, we will detail the adaptation and implementation in our laboratory of the murine AMI model proposed by Gao et al. To our knowledge, we are at the moment the only research team in Romania that successfully uses this technique. Further, we are presenting an immunological analysis platform for the study of the innate immune response to AMI in this mouse model, as well as histological and immunohistochemical techniques for the study of revascularization and fibrosis. The mouse model and the associated techniques presented here offer a competitive platform for the future study of pathologic processes and potential therapeutic interventions aiming to improve cardiac function and recovery post-AMI.

2. MATERIALS AND METHODS

2.1 Animals

Female wild-type (C57BL6) mice, 8-12 weeks of age, 20-25 g of body weight, were purchased from the Cantacuzino National Research and Development Institute (Bucharest, RO). All animal studies were conducted at the Experimental Station of „George Emil Palade" University of Medicine, Pharmacy, Science and Technology of Târgu Mureș according to protocols approved by the Scientific Research Ethics Commission of the University. The mice were allowed to acclimatize for at least one week before being included into an experimental group. Adequate environmental conditions (temperature, humidity and ventilation) were provided according to the University's guidelines for the accommodation and care of laboratory animals. Mice were housed in cages that ensured adequate space with a 12-hour light-dark cycle and free access to water and regular mouse diet.

2.2 Protocol of permanent coronary artery occlusion

2.2.1. The surgical instruments were sterilized and placed on the operating table so that they were easily and quickly accessible at any time during the operation. Keeping the same location of the instruments for all subsequent operations to develop certain reflexes is of vital importance during the intervention (Figure 1A).

2.2.2. The mouse (generally 8-12 weeks of age and at least 20 grams body weight) was anaesthetized with 5% isoflurane combined with 1 L/minute oxygen inhalation in an inducing sealed chamber made of polycarbonate plastic to which the gaseous anesthetic was delivered by an EZ-SA800 Single Animal System (Philadelphia, USA) (Figure 1B).

2.2.3. Once anaesthetized, the mouse was moved from the inducing chamber to a heated surgical board, immobilized with tape on all 4 paws and continuously anaesthetized with 2-3% isoflurane combined with 0.5 L/minute oxygen administered through a non-invasive mask placed over the nose and mouth of the animal, connected to the same anaesthesia system (Figure 1C).

2.2.4. The fur was removed with a standard trimmer for small animals (an electric beard trimmer can also be used) and the skin was cleaned with water and thereafter with betadine and alcohol pads.

2.2.5. A small skin cut (1-1.2 cm) was made on the left side of the chest, followed by careful dissection and

retraction of the pectoral major and minor muscles to expose the 4th intercostal space as shown in Figure 1F. It is very important that the pectoral muscles remain intact, because they are necessary to cover the opening (the mini-thoracotomy) once the heart has been returned into the thorax.

2.2.6. A small window was made at the 4th intercostal space level with a curved mosquito clamp to open the pleural membrane and pericardium (Figure 1G). With the clamp slightly open and by gently pressing on the opposite side of the chest, the heart was smoothly "popped out" of the thorax through the small intercostal opening.

2.2.7. In the shortest possible time, the LAD was visually located (in the region between the terminal branches of the left cardiac vein - left and lower limit, left atrial appendage - upper limit, right ventricle - right limit) and ligated at approximately 2-3 mm from the origin by using a 6.0 silk suture (Figure 1H-1J). The ligation was deemed successful when the anterior wall of the left ventricle turned pale. Important care was taken not to puncture the right ventricle as it causes a massive hemorrhage. Silk thread is preferable because it better prevents the loosening of the ligature compared to the synthetic thread. This surgical step should be performed as quickly as possible, as increasing the

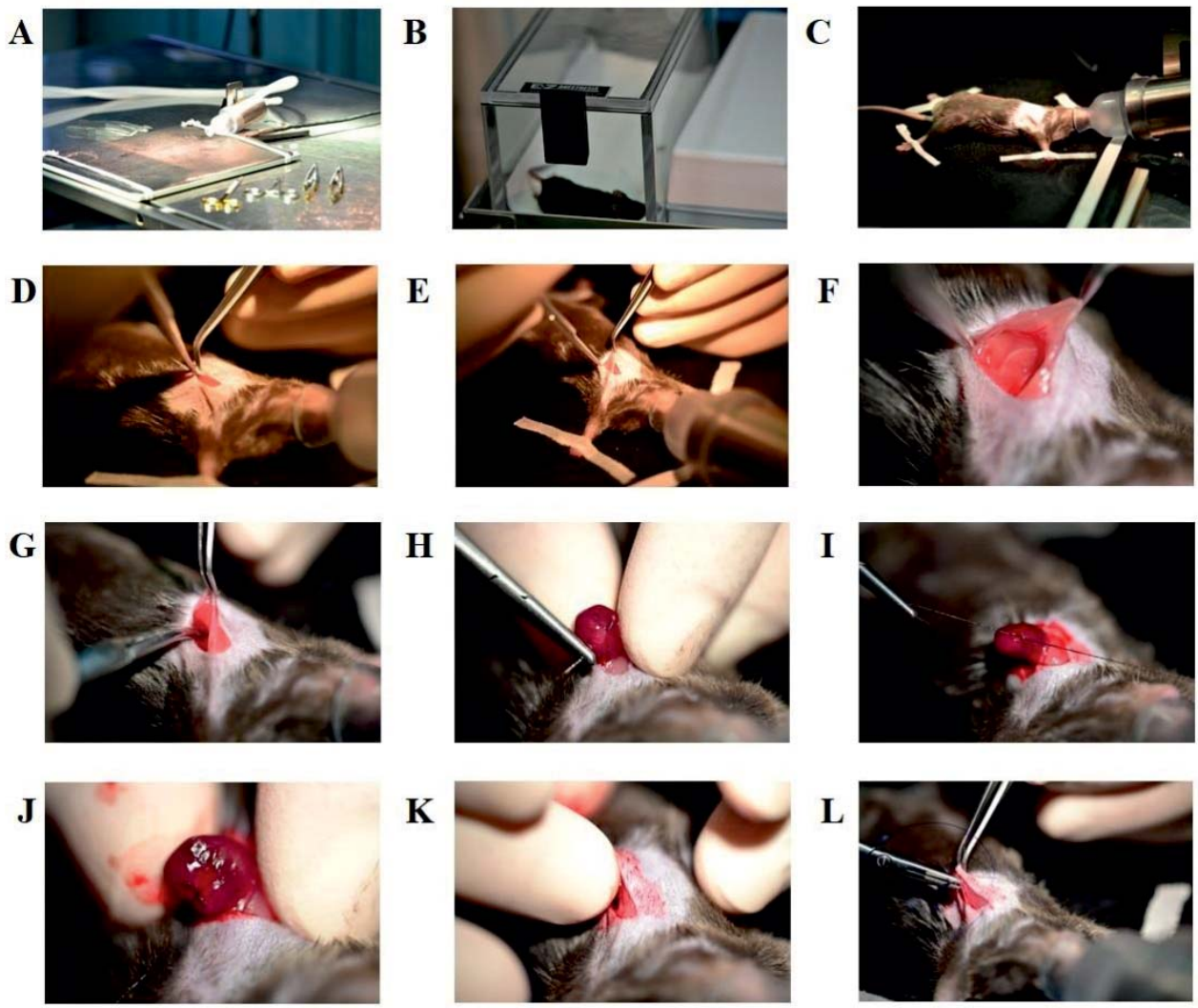

Figure 1. Permanent coronary artery occlusion without mechanical ventilation in mice.
Images show the schematic presentation of the surgical technique. **A,** Preparing the operating table. **B,** Anesthetizing the mouse in the induction chamber. **C,** Placing the unconscious mouse on a warm pad and removing the fur from the chest. **D,** Making a small skin cut in the middle position of precordial chest. **E,** Dissecting and retracting the pectoral major and minor muscles. **F,** Exposing the 4th intercostal space. **G,** Placing the curved mosquito clamp at the 4th intercostal space level with the help of a forceps and forcing the mosquito to open the pleural membrane and pericardium. **H–J,** Smoothly and gently lifting out the heart through the window, locating and ligating the LAD with silk suture. **K,** Placing the heart back into the thorax promptly after ligation, with manual evacuation of air by gentle but efficient side chest pressure. L, closure of the skin with Prolene suture.

time required for this step to over 30 seconds significantly decreased the survival rate in our experiments.
2.2.8. The heart was re-inserted into the thorax, the pneumothorax was evacuated by gentle bilateral side pressure, the pectoral muscles were layered again to cover the incision, and the skin was closed with 6.0 Prolene suture (Figure 1K-1L).
2.2.9. The mouse was disconnected from the isofluorane inhalator and allowed to breathe room air and monitored on a heating blanket until recovery. No invasive artificial respiratory aid was required. Parenteral analgesia with one dose of buprenorphine (0.1 mg/kg) was administered subcutaneously immediately after the incision was closed. The mouse usually regained consciousness within 3 minutes.
2.2.10. After completion of the surgical procedure, the mice were connected to a continuous three-lead electrocardiogram (ECG) monitoring device (Small Animal Physiological Monitoring System, Harvard Apparatus, United States) and the success of the intervention was determined by changes in the morphology of the QRS complexes (Figure 2).
2.2.11. After the surgical intervention, the surgical tools were cleaned with water and alcohol.

2.3 Histological and immunohistochemical analysis

Histological analyses of heart sections were performed at 1, 3, 7 and 14 days after AMI induction. To collect the heart, the mouse was anesthetized by intraperitoneal injection of ketamine at a dose of 80 mg/kg. If needed for biochemical or flow cytometry measurements, blood was collected by opening the thorax and puncturing the left and then the right ventricle with a heparinized 1mL syringe with a 26G needle. To heparinize the syringe, we drew and ejected a heparin solution once. A volume of 10mL of the same heparin solution was also added to the collection tubes, to prevent blood coagulation. After blood collection, the coronary and systemic vasculature were perfused with 5-10mL of PBS or 0.9% NaCl by left ventricle apical puncture (after first cutting a liver lobe to allow the extravasation of blood and perfusion fluid) and the hearts were harvested and fixed in 4% formalin for 24 hours at room temperature. The perfusion step is important in order to remove blood cells from the coronaries. The formalin-fixed tissues were processed and embedded in paraffin using routine histological procedures. Hematoxylin and eosin (H&E) and Masson's trichrome kits were purchased from Sigma-Aldrich (MO, USA) and used as described in the protocol of the manufacturer. The hearts were serially sectioned in 4µm-thick sections at several levels along the transversal axis, starting at the apex and ending at the level of the ligature. Up to 10 slides (3 sections per slide) were collected from each level. The first slide of the second level of sectioning was started 300µm from the first slide of the first level, and so on. Generally, 5-6 levels were obtained from each heart, covering approximately 1.5-2mm. For each marker, we stained one section from all 5-6 levels.

Hematoxilin eosin staining was used to visualize the inflammatory infiltrate and cardiomyocyte loss secondary to acute ischemia. Masson's Trichrome staining was used to stain collagen fibers, in order to evaluate the extension of fibrosis in the infarcted myocardium. Primary antibodies against S100A8/A9, CD31 and alfa-smooth muscle actin (α-SMA) were purchased from Cell Signaling Technology (Danvers, MA, USA). S100A8/A9 is a pro-inflammatory alarmin that increases rapidly in the infarcted myocardium. S100A8/A9 is produced in large quantities by neutrophils but also by activated monocytes and macrophages[10]. We

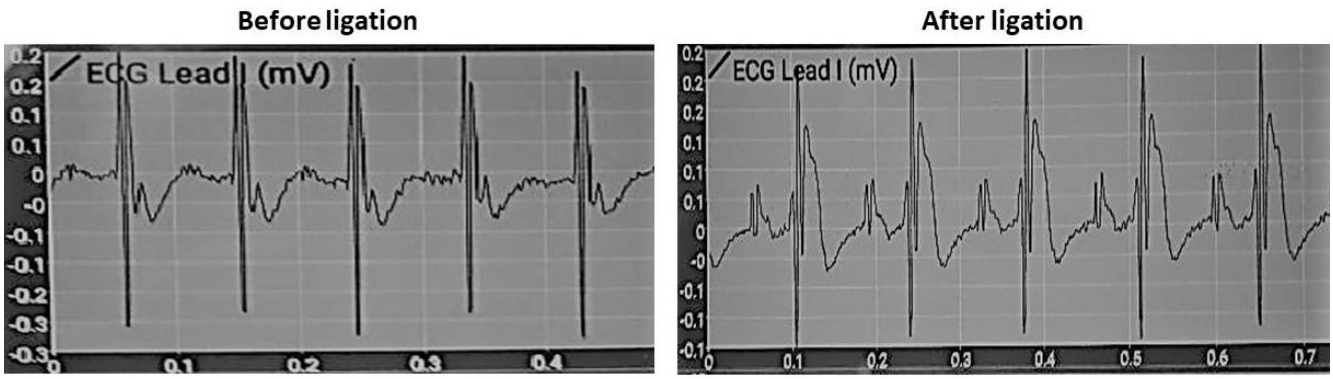

Figure 2. Validation of LAD ligation by electrocardiography
Elevations of the S-T segment appear a few minutes after LAD ligation, confirming the successful induction of ischemia.

used immunohistochemical staining of the endothelial cell marker CD31 to visualize capillaries in the infarcted and remote myocardium. α-SMA is a marker used to identify mature myofibroblasts. BrightVision Poly-HRP-Anti Rabbit Biotin-free (ready-to-use) from Immunologic (a WellMed Company, Duiven, The Netherlands) was used as secondary antibody. Images were acquired on an Axio Imager Z2 microscope with a color Axiocam 506 camera and processed using the ZenPro 3.2 software (all Zeiss, Germany) and QuPath (https://qupath.github.io).

2.4 Cell isolation for flow cytometry

In separate experiments, after the mice were sacrificed and perfused as above, the heart was rapidly removed and stored in PBS tubes kept on ice. The heart was minced in small parts with scissors (or scalpel) and enzymatically digested by a solution containing collagenase type I (2 mg/ml), collagenase type XI (0.2 mg/ml), deoxyribonuclease (DNase) type I (0.16 mg/ml), and hyaluronidase type I-S (0.14 mg/ml), all reagents from Sigma-Aldrich. The incubation time was one hour at 37°C, shaken at 230 rotations per minute. Cell suspensions were sequentially filtered through 70µm and 50µm cell strainers to remove debris. For blood analysis, the samples were collected in pre-heparinized tubes by left and right ventricle apical puncture and kept on ice, as described above.

2.5 Flow cytometry

The protocol for cell isolation and flow cytometry staining is an adapted version of the protocol used in our previous publications[11,12]. Cells from blood and heart were collected at 1, 3 and 7 days after AMI and analyzed by flow cytometry. After tissue digestion, cells from individual hearts were resuspended in 50mL of staining buffer (1% fetal calf serum, 0.05% sodium azide in PBS), centrifuged at 1500 RPM for 5 minutes, resuspended in 250µL of staining buffer, and then split into five samples of 50µL from each heart (of which 3 samples were used to stain the leukocyte populations mentioned below). Circulating cells were stained in tubes with 50µL blood. Leukocytes (neutrophils, monocytes and macrophages) were stained by adding the antibody mix into the tubes containing 50µL heart cell suspension or 50µL blood, followed by incubation in the dark at 4°C for 40 minutes, and 3 washing steps with staining buffer. The following antibodies were used, diluted 1:200 before being added into the samples: Pacific Blue (PB)-conjugated anti-mouse CD45 antibody, Allophycocyanin/Cyanine 7 (APC/Cy7)-conjugated anti-mouse CD11b antibody, Phycoerythrin (PE)-conjugated anti-mouse Ly6-G antibody, PE-conjugated anti-mouse CD115 antibody, Peridinin-Chlorophyll-Protein-Cyanine 5.5 (PerCP-Cy 5.5)-conjugated anti-mouse Ly6-C antibody, Allophycocyanin (APC)-conjugated anti-mouse F4/80 antibody, PE-conjugated anti-mouse MerTK antibody (all reagents from BioLegend , San Diego, CA, USA). After staining of blood cells, erythrocyte lysis was performed with BD FACS™ Lysing Solution (BD Biosciences, San Jose, CA, USA). Cells were washed three times, resuspended in 500µL of staining buffer and immediately analyzed. All reagents were purchased from BD PharMingen (San Diego, CA, USA). Identification of cellular populations in the antibody-stained cell suspensions was performed with a FACSAria II Flow Cytometer (BD Biosciences, San Jose, CA, USA). Data were acquired until 100.000 events were collected in the live cell gate, defined by using the forward/side scatter plots. The live cell gate was set to exclude events with low forward scatter signals, which are most likely cellular debris (Figure 5 Aa, Ba and Ca). The FlowJo software (BD Biosciences, San Jose, CA, USA) was used for data analysis and flow cytometry plot design.

3. RESULTS

3.1 AMI induction was successfully validated by ECG

We examined the changes in the morphology of the QRS complexes by continuous three-lead ECG monitoring. As shown in Figure 2, the S-T segments were markedly elevated in mice after LAD ligation. These changes appeared within the first 3 minutes of ischemia, thereby confirming AMI induction. A successful surgery is characterized by a total surgical procedure time of up to 3 minutes, with a heart exposure time for LAD ligation of up to 20 seconds. The time to full recovery of the animals after cessation of inhalatory anesthesia was up to 5 minutes. In the hands of an experienced operator, the short-term post-operative animal survival reached up to 80%, and the long-term survival rate (from 1 hour after surgery until harvest) was up to 95%. The overall survival rates (including surgery-related death) were about 65-75%, which is in accordance with the existing literature[9].

3.2 The histological features and timeline characterization of the infarcted myocardium

We developed histological and immunohistochemical methods to assess the timeline of the local changes induced by ischemia to the local environment of the

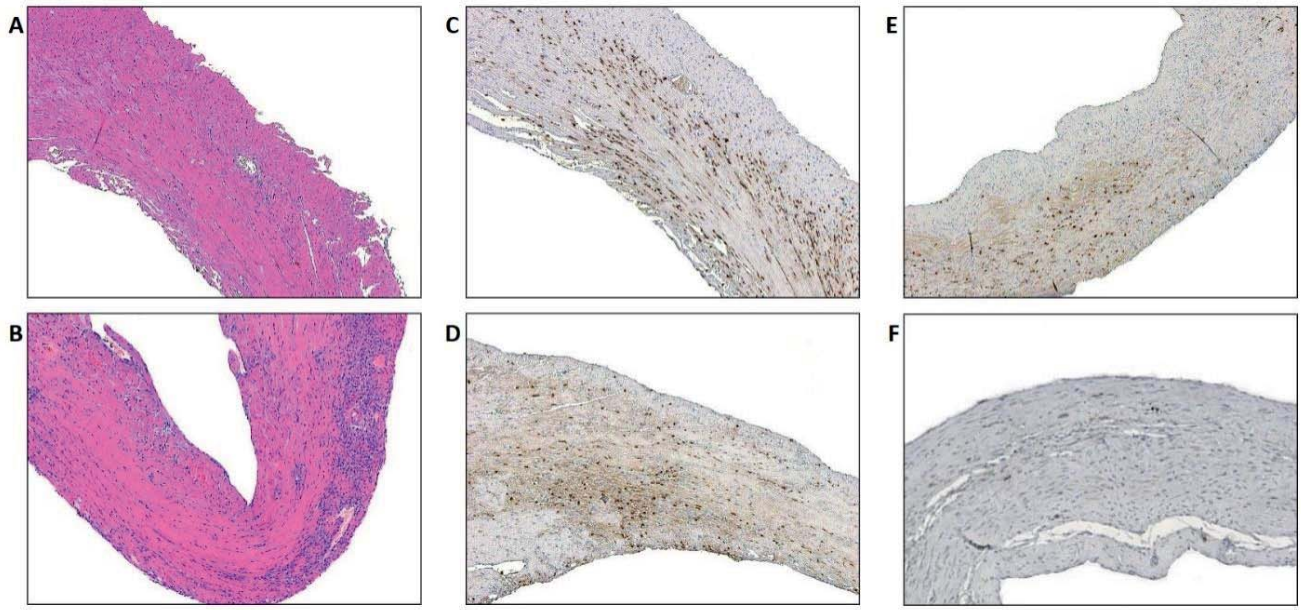

Figure 3. Inflammatory infiltration post-AMI determined by histology and immunohistochemistry
A, H&E at day 1 after AMI. **B,** H&E at day 3 after AMI. **C,** S100A8/A9 positive cells at day 1 after AMI. **D,** S100A8/A9 positive cells at day 3 after AMI. **E,** S100A8/A9 positive cells at day 7 after AMI. **F,** S100A8/A9 positive cells at day 14 after AMI. All 10X magnification.

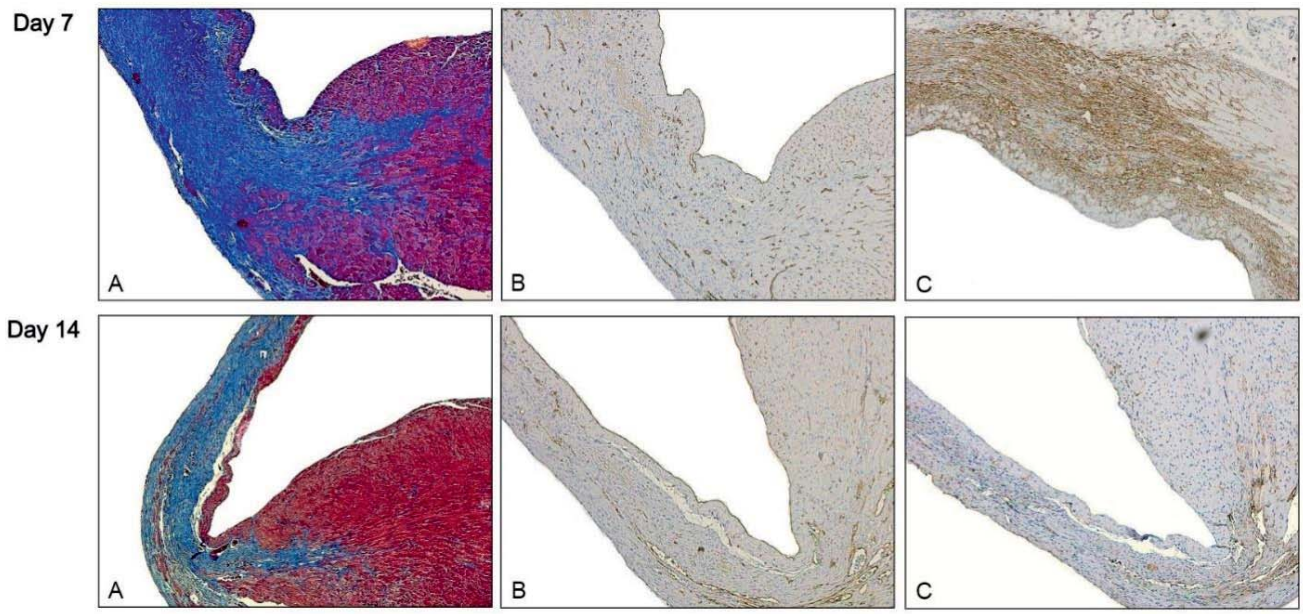

Figure 4. Fibrous scar formation, neovascularization and myofibroblast presence at 7 and 14 days after AMI
A, Masson's trichrome staining. **B,** CD31 positive cells. **C,** α-SMA positive cells. All 10X magnification.

myocardium. Myocardial necrosis triggers an acute inflammatory reaction that is maximal during the first 3 days. In the hematoxylin-eosin staining presented in Figure 3A-3B, we can observe a massive infiltration of inflammatory cells that progresses from day 1 to day 3. Interestingly, the inflammatory infiltration does not only occur in the infarcted area (central), but also in the nearby and remote myocardium (Figure 3B, up-

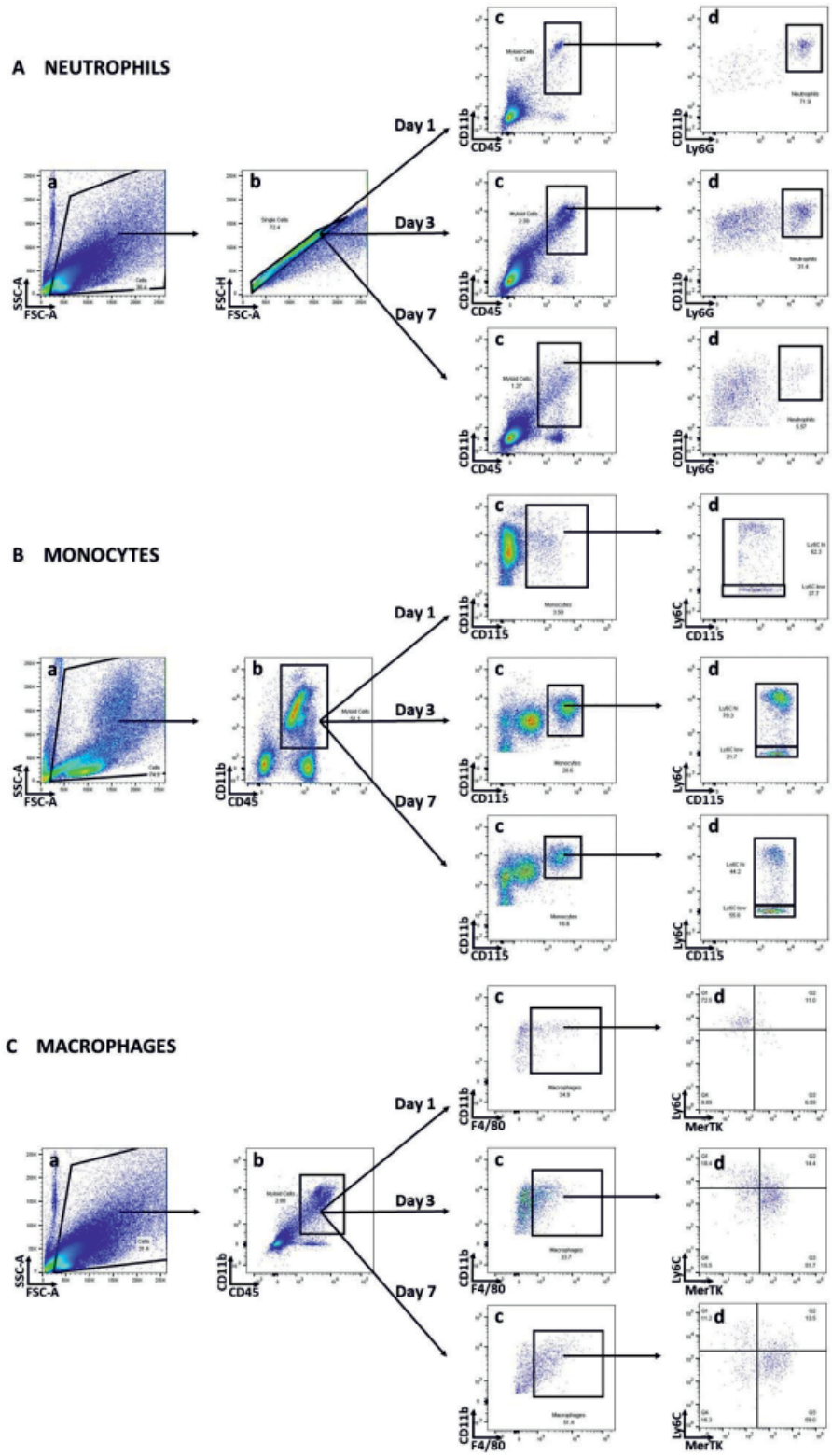

Figure 5. Inflammatory cells dynamics after AMI and the flow cytometry gating strategy
A, neutrophils in the infarcted myocardium at 1, 3 and 7 days after AMI. (a), (b) single cells selection using the forward scatter/side scatter plots. (c) myeloid cells ($CD45^+CD11b^+$) derived from the single cells gate. (d) Ly6G/CD11b plot to identify neutrophils ($CD45^+CD11b^+Ly6G^+$). **B,** monocytes in blood at 1, 3 and 7 days after AMI. (a) cells selection using forward/side scatter plots, to eliminate debris. (b) myeloid cells. (c) CD115/CD11b plot identifying total monocytes ($CD45^+CD11b^+CD115^+$ cells). (d) CD115/Ly6C plot to divide monocytes into inflammatory $Ly6C^{hi}$ monocytes (upper gate) and patrolling $Ly6C^{low}$ monocytes (lower gate). **C,** macrophages in the infarcted myocardium at 1, 3 and 7 days after AMI. (a) cells selection using forward/side scatter plots. (b) myeloid cells. (c) F4/80/CD11b plot identifying total macrophages ($CD45^+CD11b^+F4/80^+$ cells). (d) MerTK/Ly6C gate to identify the reparatory $Ly6C^{low}MerTK^{hi}$ macrophages (right lower quadrant) and inflammatory $Ly6C^{hi}MerTK^{low}$ macrophages (left upper quadrant).

per left corner), which may have important negative effects on the regions of the heart which have not been affected by the infarction (Figure 3A-B). The detailed identification of the different inflammatory cell populations by flow cytometry is presented below.

Besides the inflammatory infiltrate, at this stage we can observe microscopic aspects of interstitial oedema as blank spaces between the cells, even among the remote cardiomyocytes. We also observed nuclear pycnosis, as well as loss of cardiomyocyte nuclei and striations, all features of cardiomyocyte necrosis. In addition, we found an intense infiltration of S100A8/A9 in the infarcted area and in the remote myocardium (Figure 3C-F). The staining was both cellular and extracellular, suggesting S100A8/A9 secretion from the cells into the surrounding tissue. The S100A8/A9 infiltration reached a maximum on day 3 (Figure 3D), and then progressively decreased until day 14. On day 14 post-MI, S100A8/A9 was no longer detectable in the myocardium (Figure 3F). Myocardial thinning already occurs on day 7 after the onset of ischemia, due to removal of dead cardiomyocytes, which are replaced by fibrous tissue with a lower volume. The extent of myocardial fibrosis was detected by Trichrome Masson staining on days 7 and 14 post-AMI (Figure 4A). The preserved myocardium is colored in red, and the fibrous tissue in blue. Here, we present the border zone between infarcted and healthy myocardium (Figure 4A).

Additionally, on days 7 and 14 we could observe large fully endothelialised blood vessels forming in the border zone between the infarcted myocardium and the remote myocardium (Figure 4B). We also detected an important infiltration of mature myofibroblasts expressing α-SMA in the infarction zone and in the border zone (Figure 4C). Myofibroblasts synthesize type I collagen that strengthens the infarcted area and prevents rupture, forming the post-AMI myocardial scar. Both bone marrow-derived fibroblasts and myofibroblasts, as well as a TGFβ1-driven conversion of epicardial-derived cells (resident fibroblasts) into collagen-secreting myofibroblasts have been described[13]. By using the above techniques, the effects of therapeutic or experimental interventions on the infiltration of inflammatory cells, neovascularization, myofibroblasts, and fibrosis can be individually assessed in the infarcted area, remote myocardium and in the border zone.

3.3 Local and systemic analysis of the innate immune cell dynamics by flow cytometry

We analysed by flow-cytometry the immune cells from blood and heart at various time-points during the first week post-AMI. CD45, a pan-leukocyte marker, was used to identify the immune cells and to estimate the percentages of circulating and heart-infiltrating leukocytes. The surface marker CD11b was used to further discriminate cells of myeloid origin (Figure 5 Ac, Bb, Cb). Neutrophils were characterized by the presence of high levels of the lymphocyte antigen 6G (Ly6G), as previously described[14,15]. Monocytes were identified by the expression of surface CD115 and were divided into two distinct populations according to the expression levels of the lymphocyte antigen 6C (Ly6C) on their surface. The classical or inflammatory monocyte subset have high levels of Ly6C (Ly6C^{hi}) and the non-classical or patrolling subset are Ly6C^{low} [16]. Macrophages were identified as F4/80+ cells, as described in the literature[17]. In addition, according to Wan E et al[18], we identified reparatory macrophages expressing the myeloid-epithelial-reproductive tyrosine kinase receptor (MerTK) on their membrane. MerTK is an important efferocytosis receptor that mediates the uptake and clearance of dead or dying cardiomyocytes by the reparatory macrophages that infiltrate the myocardium. Based on surface markers, reparatory macrophages are defined as Ly6C^{low}MerTK^{hi}, and their Ly6C^{hi}MerTK^{low} counterparts are considered to be inflammatory.

The serial gating presented in Figure 5 shows a massive infiltration of neutrophils (CD45$^+$CD11b$^+$Ly6G$^+$ cells) into the heart in the first 3 days post-AMI. The percentage of neutrophils out of the total myeloid cell population (CD45$^+$CD11b$^+$) peaked on day 1 after infarction (Figure 5A-d) and massively decreased by day 7 (71.9% on day 1 vs. 5.57 % on day 7, Figure 6A), revealing the importance of neutrophils in the immediate inflammatory phase post-AMI.

Further, the ischemic injury led to a progressive increase in the number of monocytes (CD45$^+$CD11b$^+$CD115$^+$cells) in the blood stream, with a peak on day 3 (Figure 5B, Figure 6B). Importantly, the inflammatory Ly6C^{hi} sub-population constituted the overwhelming majority of monocytes at this stage (Figure 5 B-d, Figure 6C). As shown in other studies19, the inflammatory Ly6C^{hi} monocytes are recruited from the blood stream into the heart post-AMI and differentiate into monocyte-derived macrophages, involved in both the inflammatory and the reparatory phases of the cardiac immune response to AMI.

Consequently, we examined the presence of macrophages ($CD45^+CD11b^+F4/80^+$ cells) in the myocardium during the first week post-AMI. Our analysis has shown a progressive accumulation of macrophages into the heart, from day 1 to day 7 (Figure 5C, Figure 6D). By day 7 post-AMI, the vast majority of macrophages acquired a reparatory phenotype, characterized by high surface expression of the efferocytosis receptor MerTK (Figure 5 C-d and Figure 6E), while the percentage of inflammatory $Ly6C^{hi}MerTK^{low}$ macrophages was much lower (Figure 6F).

4. DISCUSSION

Despite remarkable progress in reducing mortality from AMI in recent decades by streamlining myocardial reperfusion strategies and antithrombotic therapies, innovative therapies are still needed in order to maximize the survival and prognosis of AMI patients. Early studies suggesting that inflammation is deleterious and has a considerable impact on long-term prognosis have stimulated great interest in developing beneficial anti-inflammatory strategies in AMI patients[20,21]. The reliance on animal models of cardiovascular disease is a mandatory path to follow for a better understanding of disease pathophysiology and for testing of any kind of therapeutic approach. Experimental ischemia can be induced by ligating the coronary arteries, and since the first mouse AMI model was published[8], LAD ligation has been considered as a standard model to induce myocardial ischemia and infarction. The initi-

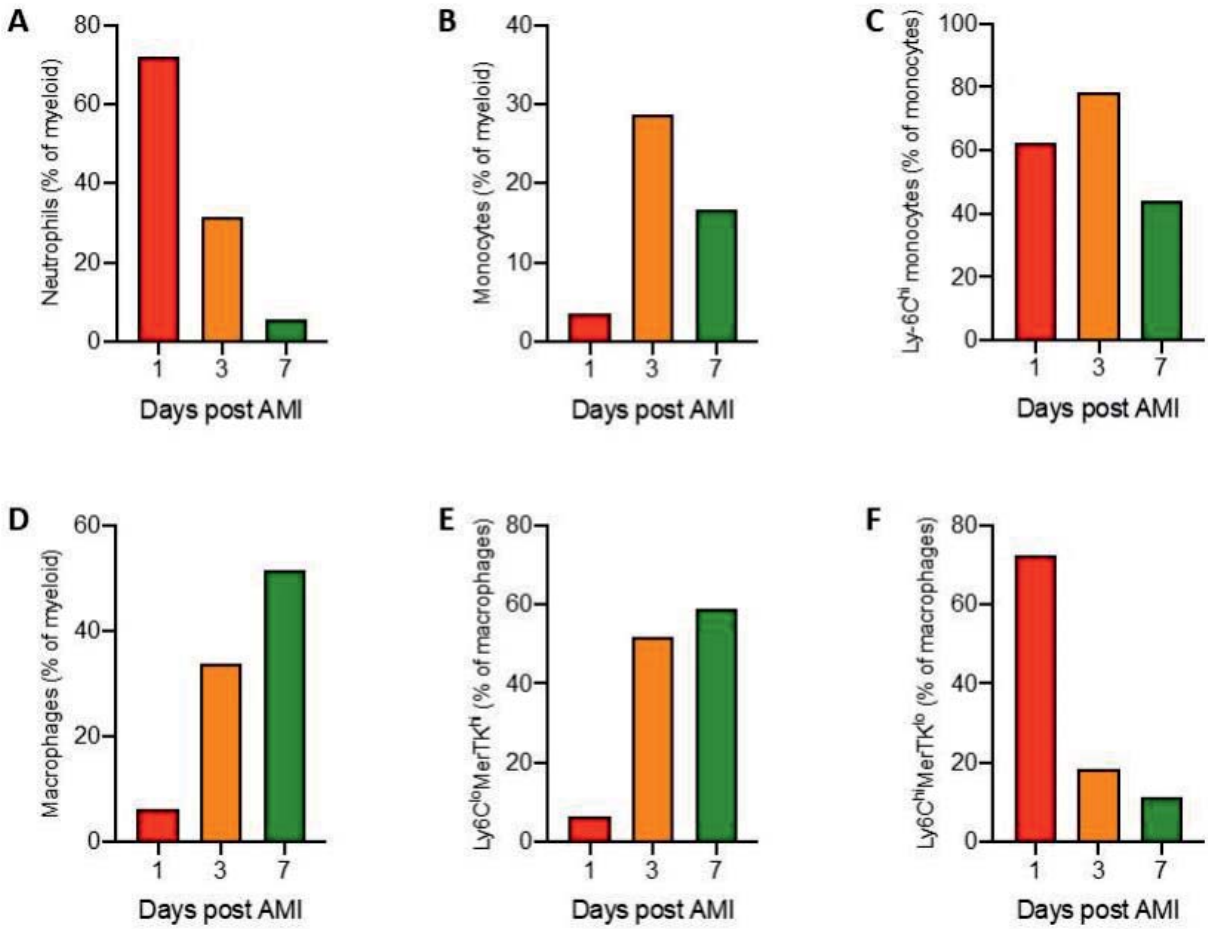

Figure 6. Immune cell dynamics post-AMI in blood and myocardium during the first week post-AMI, determined by flow cytometry
Percentages of: **A,** neutrophils in the infarcted myocardium out of total myeloid cells. **B,** circulating monocytes out of total myeloid cells in blood. **C,** inflammatory Ly6Chi monocytes out of total blood monocytes. **D,** macrophages in the infarcted myocardium out of total myeloid cells. **E,** reparatory $Ly6C^{lo}MerTK^{hi}$ macrophages in the infarcted myocardium out of total macrophages. **F,** $Ly6C^{hi}MerTK^{lo}$ macrophages in the infarcted myocardium out of total macrophages.

ally-employed procedure to ligate LAD in mice involves a large intercostal thoracotomy, requiring tracheal intubation and mechanical ventilation to keep the animal alive[22,23]. Access and ligature of the coronary artery is done through a large thoracic opening and the entire procedure takes up to 1 hour. During this entire period, the mouse has to be sedated and mechanically ventilated. After surgery, the mouse has to be weaned off the ventilator under close supervision until it regains spontaneous breathing, a process that can take between 30 minutes to a few hours. The main downside of this traditional model is the requirement for long-term parenteral general anesthesia, intubation and use of an external ventilator. The procedure causes extensive tissue damage, is associated with high mortality due to intubation and ventilation, and is very time consuming.

Here, we described the implementation in our laboratory of a minimally invasive approach initially proposed by Gao et al.[9], and we propose a complex model of histological, immunohistochemical, and flow cytometry analyses to evaluate the immune response post-MI. This surgical method is more efficient to induce AMI and causes less injuries compared to the classic procedure, as it is minimally invasive and does not require invasive mechanical ventilation and long-term parenteral anesthesia. The method leads to a major decrease of intra-operative and post-operative recovery times along with an increase in short- and long-term survival rates[9]. When performing the procedure, there are several important details that in our experiments have been proven to be crucial in obtaining favorable results. It is very important to ligate the LAD at the same anatomical region in all mice, 1 to 3 mm distal of the left atrium. This ensures that large infarctions of similar sizes are induced in all animals. However, differences in the infarction size will still occur due to natural variations in the coronary tree anatomy even in same-sex siblings. Failed surgery is characterized by missing the coronary artery, which will not generate an infarction and will only lead to myocardial damage from the suture. These failed cases can be identified during the histological examination as small infarction-like areas exclusively located at the same level as the suture. The success rate depends on the operator and increases with the level of experience. The successful infarctions are rather large, usually extend to the apex, and decrease in size when they approach the suture level, as they follow the anatomy of the irrigated territory. Large infarctions extend throughout the ventricular wall, and smaller infarctions usually have a central location, located in the middle of the wall thickness. Monitoring the ST segment elevation on ECG after the procedure allows to confidently exclude non-infarcted mice from the study groups. We also observed that short-term death within the first hour post-AMI is usually due to surgical errors or very large infarct size and is the main factor that impairs overall survival rate. Conversely, even in the case of induction of a large infarction, the long-term survival rate (from 1 hour after surgery until harvest) is excellent if the surgery is performed properly and fast (LAD ligation time within 30 seconds). Besides, care should be taken to minimize disturbing animals during the period when myocardial rupture may be triggered by stress, particularly at days 1–7 post-AMI. Ultimately, especially when practicing the model, we strongly recommend the researchers to perform autopsies for all prematurely dead mice in order to evaluate the potential cause of deaths. The early deaths usually occur due to technical issues such as excessive blood loss into the thorax, potentially caused by injuries to large vessels of the thorax wall or mediastinum, or lung injuries. Later deaths are usually due to AMI complications such as cardiac wall rupture or heart failure.

Integrating this AMI animal model in our platform allowed us to further investigate the histological changes induced by myocardial ischemia and to perform an in-depth analysis of tissue and blood cellular populations by flow cytometry. The local inflammatory infiltrate following an AMI has a crucial influence on both the size of the injury and on the efficiency of the reparatory mechanisms that determine myocardial remodeling and post-AMI prognosis[24]. The myocardial ischemia followed by necrosis triggers a potent immune reaction involving two mechanistically distinct phases: the inflammatory phase and the reparatory phase[25].

Histologically, we showed that in the initial inflammatory phase (the first 3 days after AMI) the infarcted myocardium was massively infiltrated by inflammatory cells, mainly consisting of neutrophils[11]. The flow cytometry analysis revealed a robust initial influx of Ly6G+ neutrophils into the infarcted myocardium, followed by a marked decrease by day 7 after AMI. Importantly, the infiltration of S100A8/A9-positive cells correlated with neutrophil dynamics. Of note, S100A8/A9 (calprotectin) is a proinflammatory alarmin that is readily produced and stored in large amounts in neutrophils. S100A8/A9 has been intensively studied by our group in recent years, with promising results as a potential

therapeutic target after AMI[11,12].

Following neutrophils, inflammatory monocytes form the second wave of cellular infiltration into the myocardium. We demonstrated by flow cytometry that the ischemic injury is followed by a sharp increase in the number of inflammatory Ly6C^{hi} monocytes in the blood stream, starting from day 1 after the coronary occlusion and reaching peak numbers by day 3. These monocytes infiltrate the myocardium and subsequently shift away from their pro-inflammatory phenotype to give rise to macrophages with a predominantly reparative phenotype (Ly6C^{low} macrophages)[26,27].

The early inflammatory response initiates uptake and removal of dead cardiac tissue, and paves the way for the reparative phase, which is also mediated by immune cells. The reparatory phase involves resolution of inflammation, myofibroblast proliferation, scar formation and neovascularization[28,29]. After AMI, the relatively small population of resident macrophages expands by abundant recruitment of monocytes from the blood stream. The spleen has been identified as the main reservoir supplying cells for the initial monocyte infiltration[30]. The flow cytometry gating strategy (Figure 5C) demonstrates a progressive accumulation of reparatory Ly6C^{low} macrophages starting from day 3 after AMI and increasing to day 7 (Figure 6D). Novel insights into the post-AMI healing process indicate a critical role for the efferocytosis receptor MerTK, expressed by reparatory macrophages (Figure 5C-d, lower right quadrant). In previous experimental studies, it has been shown that the absence of MerTK led to impaired efferocytosis of dying cardiomyocytes and impaired cardiac healing, leading to progressive loss of function[31]. Here, we demonstrate a progressive accumulation of CD11b^{+}F4/80^{+} macrophages in the myocardium, and a phenotype switch from a predominant Ly6C^{hi}MerTK^{low} population on day 1, to a population of Ly6C^{low}MerTK^{hi} cells on day 7, which clearly dominate the macrophage infiltrate (59 % out of total macrophages, Figure 5C-d, 5C-e, 6D-F).

The extent of the myocardial damage, as revealed by the fibrous scar, can be visualized by tissue staining with Masson's trichrome starting 5-7 days after injury (Figure 4A). This proliferative phase of the infarct healing is characterized by expansion and activation of the cardiac fibroblast population, which acquire a myofibroblast phenotype characterized by expression of alfa-smooth muscle actin (α-SMA) and produce the collagen fibres that form the scar (Figure 4B-4C). This stage is also characterized by stimulation of angiogenesis (Figure 4B). Importantly, the reparatory macrophages are critical stimulators of the fibrogenic and angiogenic responses[32]. In experimental models of AMI, depletion of macrophages causes severe reparative defects associated with impaired fibroblast activation and attenuated angiogenesis[33]. Here, we demonstrate that robust neoangiogenesis occurs, especially in the border zone between the infarcted and the remote myocardium.

The resolution of inflammation and initiation of fibrosis are finely tuned processes aiming to limit the inflammatory myocardial damage and lead to optimal healing. However, as the reparatory macrophage accumulation is dependent on the initial inflammatory activation, all interventions that inhibit the initial inflammatory response invariably affect the reparatory phase as well. Affecting the timing and magnitude of the inflammatory response can help reduce the inflammatory damage but can also impair the adequate wound healing process. For example, we have shown that pharmacological blockade of the S100A8/A9 alarmin has important therapeutic benefits when administered during the inflammatory phase of the AMI but led to impaired repair and cardiac dysfunction when given long-term[10,11]. Therefore, care should be exercised when developing immunomodulatory therapies for AMI and the effects on both phases of the immune response should be carefully considered.

5. CONCLUSION

The innate immune system plays a critical role in the repair and remodeling of the infarcted myocardium. An initial inflammatory phase is required to recruit the cells that repair the myocardium, but excessive inflammation leads to further damage. In contrast, a weakened inflammatory phase leads to inefficient repair and also affects function. These are very important aspects that have to be taken into consideration by all attempts to develop anti-inflammatory therapies for AMI.

The AMI model described here, alongside the subsequent tissue and cellular analyses, is an important tool that supports the understanding of the role of the immune system in AMI and the testing of novel therapeutics approaches. Any potentially successful immunomodulatory therapy would have to limit the inflammatory damage to the myocardium, while improving or keeping intact the reparatory mechanisms.

Compliance with ethics requirements:

The authors declare no conflict of interest regarding this article. The authors declare that all the procedures and experiments of this study respect the ethical standards in the Helsinki Declaration of 1975, as revised in 2008(5), as well as the national law. Informed consent was obtained from all the patients included in the study.

Financial support: This work has been supported by a project grant awarded by the Ministry of Research and Innovation of Romania, CNCS-UEFISCDI (National Council of Scientific Research - Executive Unit for Financing Higher Education and Innovation), project number PN-III-P4-ID-PCCF-2016-0172, within PNCDI (National Research, Development and Innovation Plan) III. „George Emil Palade" University of Medicine, Pharmacy, Science and Technology of Targu Mures has also granted financial support by funds from the doctoral scholarship.

References:

1. Yeh RW, Sidney S, Chandra M, Sorel M, Selby JV, Go AS. Population trends in the incidence and outcomes of acute myocardial infarction. N Engl J Med 2010;362: 2155–65.
2. Nielsen PH, Maeng M, Busk M, Mortensen LS, Kristensen SD, Nielsen TT, Andersen HR. Primary angioplasty versus fibrinolysis in acute myocardial infarction: long-term follow-up in the Danish acute myocardial infarction 2 trial. Circulation 2010;121: 1484–1491.
3. Zhang J, Knapton A, Lipshultz SE, Weaver JL, Herman EH. Isoproterenol-induced cardiotoxicity in Sprague-Dawley rats: correlation of reversible and irreversible myocardial injury with release of cardiac troponin t and roles of inos in myocardial injury. Toxicol Pathol. 2008;36(2):277–78.
4. Antonio EL, Dos Santos AA, Araujo SR, Bocalini DS, Dos Santos L, Fenelon G, Frnco MF, Tucci PJ. Left ventricle radio-frequency ablation in the rat: a new model of heart failure due to myocardial infarction homogeneous in size and low in mortality. J Card Fail. 2009;15(6): 540-548.
5. Ovsepyan A, Panchenkov D, Prokhortchouk E, Telegin G, Zhigalova N, Golubev E, Sviridova T, Matskeplishvili S, Skryabin K, Buziashvili U. Modeling myocardial infarction in mice: methodology, monitoring, pathomorphology. Acta Naturae. 2011;3(1): 107-115.
6. Wang D, Tediashvili G, Hu X, Gravina A, Marcus SG, Zhang H, Olgin JE, Deuse T, Schrepfer S. A Cryoinjury Model to Study Myocardial Infarction in the Mouse. J Vis Exp 2019;151: 1-5.
7. Villiers CD, Riley PR. Mouse models of myocardial infarction: comparing permanent ligation and ischaemia-reperfusion. Disease Models & Mechanisms 2020; 13: 1-5.
8. Johns TN, Olson BJ. Experimental myocardial infarction. I. A method of coronary occlusion in small animals. Ann Surg. 1954;140: 675-682.
9. Gao E, Lei YH, Shang X, Huang ZM, Zuo L, Boucher M, Fan Q, Chuprun JK, Ma XL, Koch WJ. A novel and efficient model of coronary artery ligation and myocardial infarction in the mouse. Circ Res. 2010;107: 1445-1453.
10. Pruenster M, Vogl T, Roth J, Sperandio M. S100A8/A9: From basic science to clinical application. Pharmacol Ther. 2016;167: 120-131.
11. Marinkovic G, Larsen HG, Yndigegn T, Szabo IA, Mares RG, De Camp L, Weiland M, Tomas L, Goncalves I, Nilsson J, Jovinge S, Schiopu A. Inhibition of pro-inflammatory myeloid cell responses by short-term S100A9 blockade improves cardiac function after myocardial infarction. European Heart Journal 2019;40(32): 2713-2723.
12. Marinkovic G, Koenis DS, De Camp L, Jablonowski R, Graber N, De Waard V, Carlie De Vries CJ, Goncalves I, Nilsson J, Jovinge S, Schiopu A. S100A9 Links Inflammation and Repair in Myocardial Infarction. Circ Res. 2020;127(5): 664-676.
13. Ruiz-Villalba A, Simon AM, Pogontke C, Castillo MI, Abizanda G, Pelacho, Sánchez-Domínguez BR, Segovia JC, Prósper F, Pérez-Pomares JM. Interacting resident epicardium-derived fibroblasts and recruited bone marrow cells form myocardial infarction scar. J Am Coll Cardiol. 2015;65: 2057-66.
14. Ma Y, Yabluchanskiy A, Iyer RP, Cannon PL, Flynn ER, Jung M, Henry J, Cates CA, Deleon-Pennell KY, Lindsey ML. Temporal neutrophil polarization following myocardial infarction. Cardiovasc Res. 2016;110: 51-61.
15. Horckmans M, Ring L, Duchene J, Santovito D, Schloss MJ, Drechsler M, Weber C, Soehnlein O, Steffens S. Neutrophils orchestrate post-myocardial infarction healing by polarizing macrophages towards a reparative phenotype. Eur Heart J. 2017;38: 187-197.
16. Geissmann F, Jung S, Littman DR. Blood monocytes consist of two principal subsets with distinct migratory properties. Immunity. 2003;19: 71-82.
17. Epelman S, Lavine KJ, Beaudin AE, Sojka DK, Carrero JA, Calderon B, Brija T, Gautier EL, Ivanov S, Satpathy AT, Schilling JD, Schwendener R, Sergin I, Razani B, Forsberg EC, Yokoyama WM, Unanue ER, Colonna M, Randolph GJ, Mann DL. Embryonic and adult-derived resident cardiac macrophages are maintained through distinct mechanisms at steady state and during inflammation. Immunity. 2014;40: 91-104.
18. Wan E, Yeap XY, Dehn S, Terry R, Novak M, Zhang S, Iwata S, Han X, Homma S, Drosatos K, Lomasney J, Engman DM, Miller SD, Vaughan DE, Morrow JP, Kishore R, Thorp EB. Enhanced efferocytosis of apoptotic cardiomyocytes through myeloid-epithelial-reproductive tyrosine kinase links acute inflammation resolution to cardiac repair after infarction. Circ Res. 2013;113: 1004-12.
19. Hanna RN, Carlin LM, Hubbeling HG, Nackiewicz D, Green AM, Punt JA, Geissmann F, Hedrick CC. The transcription factor NR4A1 (Nur77) controls bone marrow differentiation and the survival of Ly6C- monocytes. Nat Immunol. 2011;12: 778-85.
20. Seropian IM, Toldo S, Van Tassell BW, Abbate A. Anti-inflammatory strategies for ventricular remodeling following ST-segment elevation acute myocardial infarction. J Am Coll Cardiol. 2014;63: 1593-603.
21. Westman PC, Lipinski MJ, Luger D, Waksman R, Bonow RO, Wu E, Epstein S. Inflammation as a Driver of Adverse Left Ventricular Remodeling After Acute Myocardial Infarction. J Am Coll Cardiol 2016;67(17): 2050-60.
22. Lugrin J, Roumen Parapanov R, Krueger T, Liaudet L. Murine Myocardial Infarction Model using Permanent Ligation of Left Anterior Descending Coronary Artery. J Vis Exp 2019;150: 1-7.
23. Aisyah S, Ghafar NA, Jubri Z, Das S. Induction of Myocardial Infarction in Experimental Animals: A Review. Journal of Clinical and Diagnostic Research 2018; 12(11): 1-05.
24. Nahrendorf M, Swirski FK, Aikawa E, Stangenberg L, Wurdinger T, Figueiredo JL, Libby P, Weissleder R, Pittet MJ. The healing myocardium sequentially mobilizes two monocyte subsets with divergent and complementary functions. The Journal of experimental medicine 2007;204: 3037-3047.
25. Mares RG, Marinkovic G, Cotoi OS, Schiopu A. Innate Immune Mechanisms in Myocardial Infarction - An Update. Revista Romana de Medicina de Laborator 2018;26(1): 9-20.
26. Hilgendorf I, Gerhardt L, Tan TC, Winter C, Holderried TA, Chousterman BG, Iwamoto Y, Liao R, Zirlik A, Scherer-Crosbie M, Hedrick CC, Libby P, Nahrendorf M, Weissleder R, Swirski RK. Ly-6Chigh Monocytes Depend on Nr4a1 to Balance both Inflammatory and Reparative Phases in the Infarcted Myocardium. Circulation Research 2014;114(10): 1611-1622.
27. Kratofil RM, Kubes P, Deniset JF. Monocyte Conversion During Inflammation and Injury. Arterioscler Thromb Vasc Biol 2017;37(1): 35-42.
28. Swirski FK. Inflammation and repair in the ischaemic myocardium. Hamostaseologie 2015;35: 34-6.
29. Prabhu SD, Frangogiannis NG. The Biological Basis for Cardiac Repair After Myocardial Infarction: From Inflammation to Fibrosis. Circ Res 2016;119(1): 91-112.
30. Swirski FK, Nahrendorf M, Etzrodt M, Wildgruber M, Cortez-Retamozo V, Panizzi P, Figueiredo JL, Kohler RH, Chudnovskiy A, Waterman P, Aikawa E, Mempel TR, Libby P, Weissleder R, Pittet

MJ. Identification of splenic reservoir monocytes and their deployment to inflammatory sites. Science 2009;325: 612-6.
31. Howangyin KY, Zlatanova I, Pinto C, Ngkelo A, Cochain C, Rouanet M, Vilar J, Lemitre M, Stockmann C, Fleischmann BK, Mallat Z, Silvestre JS. Myeloid-Epithelial-Reproductive Receptor Tyrosine Kinase and Milk Fat Globule Epidermal Growth Factor 8 Coordinately Improve Remodeling After Myocardial Infarction via Local Delivery of Vascular Endothelial Growth Factor. Circulation 2016;133: 826-39.
32. Wynn TA, Vannella KM. Macrophages in Tissue Repair, Regeneration, and Fibrosis. Immunity 2016;44: 450-62.
33. Frangogiannis NG. Emerging roles for macrophages in cardiac injury: cytoprotection, repair, and regeneration. J Clin Invest 2015;125: 2927-30.